The Eleventh International Conference on
Engineering Computational Technology
23–25 August, 2022 | Montpellier, France

Proceedings of the Eleventh International Conference on
Engineering Computational Technology
Edited by B.H.V. Topping and P. Iványi
Civil-Comp Conferences, Volume 2, Paper 11.3
Civil-Comp Press, Edinburgh, United Kingdom, 2022, doi: 10.4203/ccc.2.11.3

Reduced-order constraint formulation for segment-to-segment contact in large displacement structural analysis

M.C.K. Chuo and B.A. Izzuddin

**Department of Civil and Environmental Engineering,
Imperial College London, United Kingdom**

Abstract

Contact simulation can introduce substantial computational cost and complexity to large displacement structural analysis, which by itself can already be very expensive. The inclusion of contact simulation in a complete sense entails incorporating the full expressions of the first and second derivatives of the contact potential energy to be used for the prediction of the structural response at successive iterations of the Newton-Raphson procedure. Furthermore, these expressions would have to be re-evaluated at every iteration to account for the updating of the contact region. In order to increase computational efficiency, the contact constraint formulation can be approximated to a certain level without significant compromise in accuracy. This paper proposes several approximations to the constraint formulation whereby partial expressions of derivatives are used, depending on how the projection coordinates, the gap vector, and the unit normal vector of the contact region are assumed to vary within each equilibrium step with respect to the displacement degrees of freedom.

Keywords: contact mechanics, segment-to-segment contact, large displacement, mortar method, Lagrange multiplier, finite element analysis

1 Introduction

Incorporating contact simulation into large displacement structural analysis can introduce substantial computational cost and complexity. In order to simulate surface-to-surface contact using the Lagrange multiplier method, contact elements are introduced in the form of pairings between two segments, each segment being a

discretisation unit from one of the contacting surfaces [1, 2]. Typically, the segment from the more highly refined surface mesh is designated as the 'slave' and the other the 'master'. Each contact element introduces an individual contribution to the potential energy of the system in the form of a Lagrange multiplier formulation:

$$\Pi_{\mathrm{c}} = \int_{\Gamma_{\mathrm{c}}^{\mathrm{s}}} \lambda^{\mathrm{a}}\, g_{\mathrm{n}}\, \mathrm{d}\Gamma_{\mathrm{c}}^{\mathrm{s}} \tag{1}$$

where: $\Gamma_{\mathrm{c}}^{\mathrm{s}}$ is the elemental contact region, which is a subset of the domain of the slave segment; λ^{a} is the Lagrange multiplier field over the contact region, which represents the contact pressure field, and is an interpolation of the additional, i.e. Lagrange multiplier, degrees of freedoms (DOFs) at the nodes of the slave segment; and g_{n} is the normal gap field over the contact region, which is an interpolation of the nodal displacement DOFs from both the slave and master segments. The gap function g_{n} is given by:

$$g_{\mathrm{n}} = \left\langle n \right\rangle \left\{ \bar{x}^{\mathrm{ms}} \right\} \tag{2}$$

where: $\left\langle n \right\rangle$ is the unit normal vector field; and $\left\{ \bar{x}^{\mathrm{ms}} \right\}$ is the gap vector field over the contact region, which, if evaluated at an integration point $\left\{ \zeta^{\mathrm{s}} \right\}$ on the slave segment, represents the vector from $\left\{ \zeta^{\mathrm{s}} \right\}$ to its orthogonal projection $\left\{ \bar{\zeta}^{\mathrm{m}} \right\}$ on the master segment. Figure 1 shows the projection coordinates $\left\{ \bar{\zeta}^{\mathrm{m}} \right\}$, the gap vector $\left\{ \bar{x}^{\mathrm{ms}} \right\}$, and the unit normal vector $\left\langle n \right\rangle$ for a particular integration point $\left\{ \zeta^{\mathrm{s}} \right\}$.

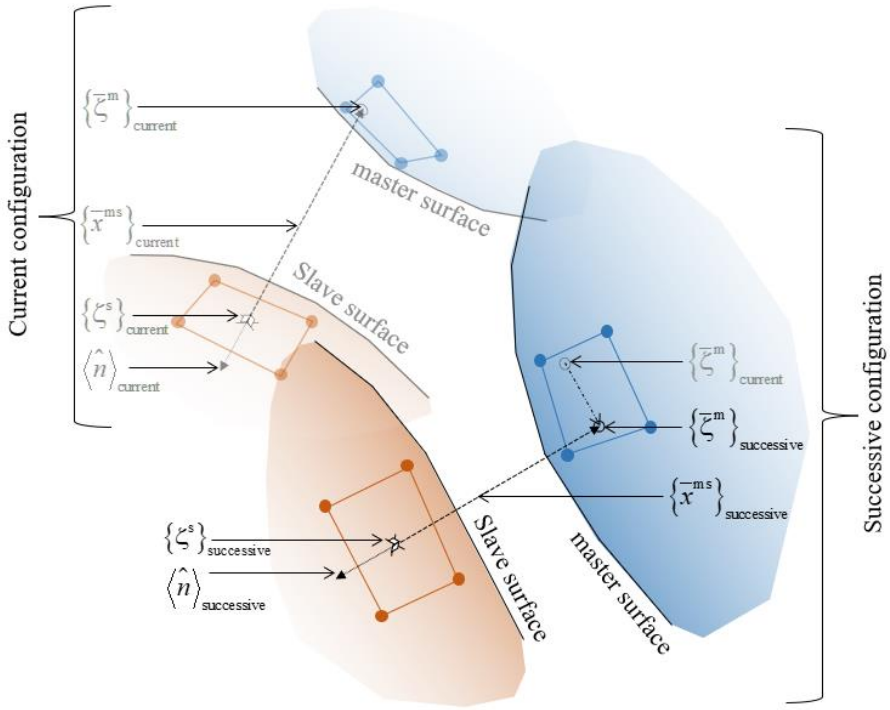

Figure 1: Projection point, gap vector, and unit normal vector for a particular integration point.

Adopting the contact constraint formulation in a complete sense would entail incorporating the full expressions of the first and second derivatives of (1) to be used for the prediction of the structural response at successive iterations of the Newton-Raphson procedure. These derivatives would then contain the first and second derivatives of $\{\bar{\zeta}^{\mathrm{m}}\}$, $\{\bar{x}^{\mathrm{ms}}\}$ and $\langle n \rangle$. A change in the set of displacements between successive iterations would invoke a change in the contact region between two contacting surfaces, hence a change in $\{\bar{\zeta}^{\mathrm{m}}\}$ as shown in Figure 1, which must be captured during the re-evaluation of the derivatives at every iteration. In the complete formulation, $\{\zeta^{\mathrm{s}}\}$ is re-projected at every iteration in order to update $\{\bar{\zeta}^{\mathrm{m}}\}$.

The contact constraint formulation can be optimised to increase the computational efficiency without significant compromise in accuracy.

2 Methods

The first aspect of the formulation optimisation is that a second-order Taylor approximation of the gap function g_{n} is taken in terms of the displacement DOFs $\{\mathrm{U}^{\mathrm{g}}\}$:

$$g_{\mathrm{n}} = g_{\mathrm{n}}\big|_0 + \delta\langle \mathrm{U}^{\mathrm{g}} \rangle \left\{ g_{\mathrm{n,g}}\big|_0 \right\} + \frac{1}{2}\delta\langle \mathrm{U}^{\mathrm{g}} \rangle \left[g_{\mathrm{n,gg}}\big|_0 \right] \delta\{\mathrm{U}^{\mathrm{g}}\} \tag{3}$$

The Taylor coefficients $g_{\mathrm{n}}\big|_0$, $\left\{ g_{\mathrm{n,g}}\big|_0 \right\}$, and $\left[g_{\mathrm{n,gg}}\big|_0 \right]$ are evaluated at the start of the equilibrium step (denoted by subscript '0'), and are not re-evaluated at every iteration. The complete expressions of $\left\{ g_{\mathrm{n,g}}\big|_0 \right\}$ and $\left[g_{\mathrm{n,gg}}\big|_0 \right]$ represent the actual first and second derivatives of g_{n} respectively, and hence contain complete expressions of the derivatives of $\{\bar{\zeta}^{\mathrm{m}}\}$, $\{\bar{x}^{\mathrm{ms}}\}$ and $\langle n \rangle$. Re-projection of $\{\zeta^{\mathrm{s}}\}$ is only done at the end of the step. The second aspect of the formulation optimisation is the approximation of $\{\bar{\zeta}^{\mathrm{m}}\}$, $\{\bar{x}^{\mathrm{ms}}\}$ and $\langle n \rangle$ based on assumptions as to whether these entities are constant, or vary linearly or quadratically with $\{\mathrm{U}^{\mathrm{g}}\}$ across the step. It is noted that the first derivative of $\{\bar{\zeta}^{\mathrm{m}}\}$ with respect to $\{\mathrm{U}^{\mathrm{g}}\}$ is an implicit function in $\{\mathrm{U}^{\mathrm{g}}\}$ obtained by the assertion that the gap vector $\{\bar{x}^{\mathrm{ms}}\}$ remains perpendicular to the slave surface over an infinitesimal change in displacement, $\delta\{\mathrm{U}^{\mathrm{g}}\}$, and its corresponding infinitesimal change in projection coordinates, $\delta\{\bar{\zeta}^{\mathrm{m}}\}$. As shown in Table 1, six 'Approximation Types' are considered here based on the different combinations of the assumptions for the variation of $\{\bar{\zeta}^{\mathrm{m}}\}$, $\{\bar{x}^{\mathrm{ms}}\}$ and $\langle n \rangle$ with respect to $\{\mathrm{U}^{\mathrm{g}}\}$.

To assess the accuracy of the different approximation types, a model is set up in ADAPTIC [2] with the initial configuration and parameters as shown in Figure *2*. Two layers, consisting of geometrically nonlinear quadrilateral solid elements with

identical dimensions, are stacked vertically. The top layer is designated as the slave layer and the bottom the master. The top faces of solid elements M1-7 are coupled with the bottom faces of S1-7 via contact elements C1-7, and hence there are no shared nodes between the two layers at this vicinity. The applied loads shown in Figure *2* are proportional loads, where the load factor γ is increased from 0 to 10 over 4 steps. The analysis is run for each approximation type adopted by the contact elements, as well as for the complete formulation. In each case, the percentage error of the strain energy at $\gamma = 10$ for Approximation Types 1-6 is calculated as follows:

$$\text{Percentage error of strain energy} = \frac{U_{\text{type}} - U_{\text{complete}}}{U_{\text{complete}}} \times 100\% \qquad (4)$$

where U_{type} is the total strain energy of the system when a particular approximation type is adopted, and U_{complete} is the total strain energy of the system when the complete formulation is adopted. The study is then repeated with 6, 8, 10, 12, 14, 16, 18, and 20 load steps.

Approximation Type	Variation of projection coordinates $\{\bar{\xi}^{m}\}$	Variation of gap vector $\{\bar{x}^{ms}\}$	Variation of unit normal vector $\langle n \rangle$
1	Constant	Linear	Constant
2	Linear	Linear	Linear
3	Linear	Quadratic	Linear
4	Quadratic	Quadratic	Linear
5	Linear	Quadratic	Quadratic
6	Quadratic	Quadratic	Quadratic

Table 1: Approximation Types with different combinations of assumptions for the variation of the entities.

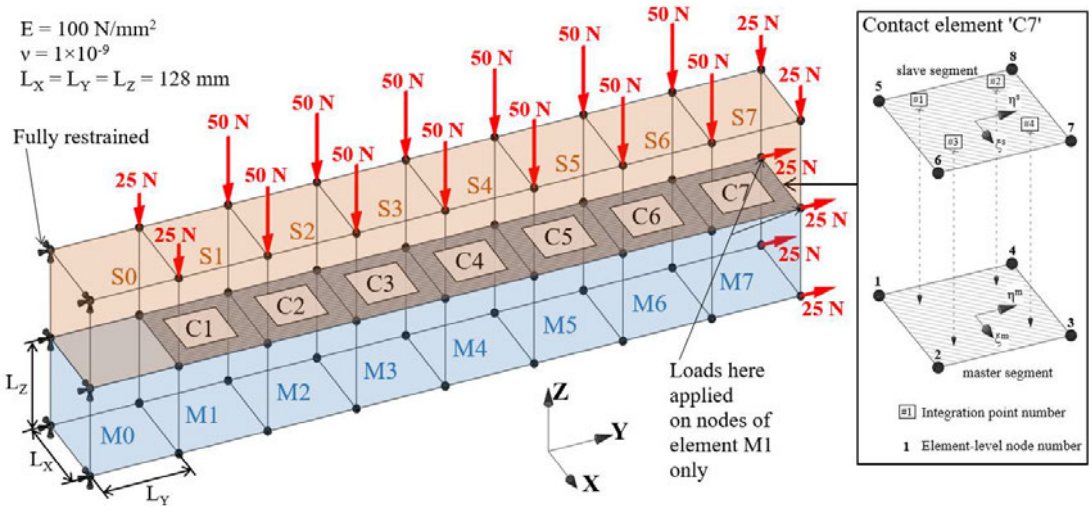

Figure 2: Numerical example with contact elements adopting the different Approximation Types.

3 Results

Figure 3(a) shows the deformed configuration at $\gamma = 10$, which is similar for all approximation types and the complete formulation. Due to the nature of the boundary conditions, the model behaves as two vertically stacked cantilever beams supported at the same end. As the free end of the cantilever deflects downwards, due to the lack of composite action between the two layers, the layers slip relative to each other in the direction of the beam axis. Furthermore, the directions of the unit normal vectors $\langle n \rangle$ of the contact elements change as well. The model configuration and applied loads are set up such that, within the maximum load factor of the study, the integration points of the slave segment of any contact element would not end up projecting into the master segment of another.

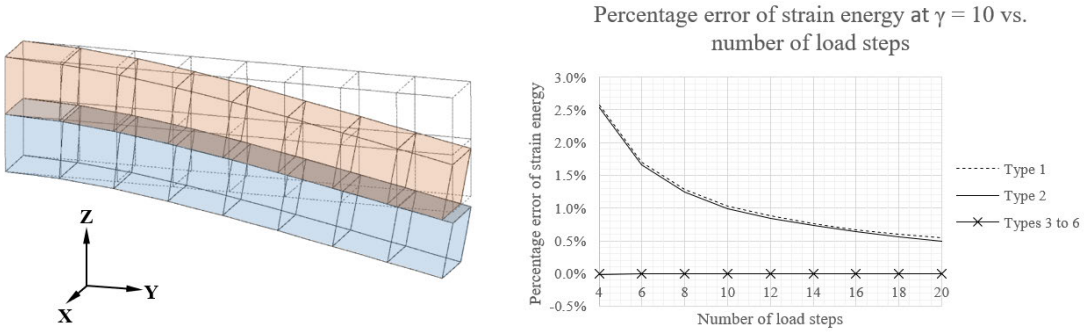

(a) (b)

Figure 3: (a) Deformed configuration of model at final load factor with displacement scale factor of 1; (b) Plot of percentage error of strain energy against number of load steps for different Approximation Types.

As shown in Figure 3(b), the percentage errors of the strain energy of the different Approximation Types converge to zero as the number of load steps increase, i.e. the size of the load step decreases. This verifies their ability to approximate the complete contact formulation. It can be seen that a very high accuracy is achieved with Approximation Type 3 onwards, having a percentage error of only -0.0011% when 4 load steps are used. This shows that it is reasonably accurate to assume a linear variation of the projection coordinates $\{\overline{\xi}^{\mathrm{m}}\}$ and the unit normal vector $\langle n \rangle$ with the displacement DOFs $\{\mathrm{U}^{\mathrm{g}}\}$, and the nonlinearity of the complete contact formulation can be captured satisfactorily as long as a quadratic variation of the gap vector $\{\overline{x}^{\mathrm{ms}}\}$ is adopted. It is noted that the quadratic variation of the gap vector $\{\overline{x}^{\mathrm{ms}}\}$ in Approximation Types 3 and 4 is also approximate in itself. This is because the full expression of the second derivative of $\{\overline{x}^{\mathrm{ms}}\}$ with respect to $\{\overline{\xi}^{\mathrm{m}}\}$ would contain the second derivative of $\{\overline{\xi}^{\mathrm{m}}\}$ as well, but this is omitted in these two Approximate Types due to the assumption of a linear variation of $\{\overline{\xi}^{\mathrm{m}}\}$.

4 Conclusions and Contributions

Approximative reduced-order constraint formulations are proposed in this paper to enhance the computational efficiency of contact simulation. In the approximate formulations, partial expressions of derivatives are used, depending on how the projection coordinates $\{\overline{\xi}^{\mathrm{m}}\}$, the gap vector $\{\overline{x}^{\mathrm{ms}}\}$, and the unit normal vector $\langle n \rangle$ are assumed to vary within each equilibrium step with respect to the displacement DOFs $\{\mathrm{U}^{\mathrm{g}}\}$. All these entities are approximated within each equilibrium step and the projection of the integration points $\{\zeta^{\mathrm{s}}\}$ onto the master surface is only employed at the end of each step, after equilibrium has been achieved. Six different 'Approximation Types' are implemented and tested here, based on different combinations of the assumptions for the variation of $\{\overline{\xi}^{\mathrm{m}}\}$, $\{\overline{x}^{\mathrm{ms}}\}$ and $\langle n \rangle$ with respect to $\{\mathrm{U}^{\mathrm{g}}\}$. It was found that good accuracy is already achieved on the assumption that both $\{\overline{\xi}^{\mathrm{m}}\}$ and $\langle n \rangle$ vary linearly and $\{\overline{x}^{\mathrm{ms}}\}$ varies quadratically with the displacement DOFs $\{\mathrm{U}^{\mathrm{g}}\}$. This circumvents the need for evaluating the second derivatives of $\{\overline{\xi}^{\mathrm{m}}\}$ and $\langle n \rangle$, which can be expensive due to their extensive formulations. Further cost savings can potentially be achieved from the fact that the entities are only re-evaluated at the start of the step instead of at every iteration. An overall reduction in the expense of computing the contact constraint formulations would expedite the problem solution, hence allowing for the conception of contact simulation models involving more complex configurations and loadings.

Acknowledgements

The authors would like to acknowledge the support of the President's Scholarship at Imperial College London for the PhD study of the first author.

References

[1] K.A. Fischer, P. Wriggers, "Frictionless 2D contact formulations for finite deformations based on the mortar method", Computational Mechanics, 36(3), 226-244, 2005. https://doi.org/10.1007/s00466-005-0660-y

[2] M.A. Puso, T.A. Laursen, "A mortar segment-to-segment contact method for large deformation solid mechanics", Computer methods in applied mechanics and engineering, 193(6-8), 601-629, 2004. https://doi.org/10.1016/j.cma.2003.10.010

[3] B.A. Izzuddin, "Nonlinear dynamic analysis of framed structures", Imperial College London, University of London, 1991.